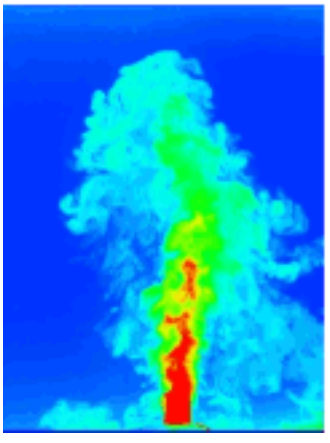

Journal of Turbulence
Publication details, including instructions for authors and subscription information:
http://www.tandfonline.com/loi/tjot20

Presentation of anisotropy properties of turbulence, invariants versus eigenvalue approaches

S. Banerjee [a] , R. Krahl [b] , F. Durst [a] & Ch. Zenger [c]

[a] Lehrstuhl für Stromungsmechanik, Cauerstrasse 4, Erlangen, 91058, Germany

[b] Lehrstuhl für Angewandte Mathematik III, Haberstr. 2, Erlangen, 91058, Germany

[c] Lehrstuhl für Informatik mit Schwerpunkt Wissenschaftliches Rechnen, Technical University Munich, Munich, Germany

Version of record first published: 02 Nov 2009.

To cite this article: S. Banerjee , R. Krahl , F. Durst & Ch. Zenger (2007): Presentation of anisotropy properties of turbulence, invariants versus eigenvalue approaches, Journal of Turbulence, 8, N32

To link to this article: http://dx.doi.org/10.1080/14685240701506896

Journal of Turbulence
Volume 8, No. 32, 2007

Presentation of anisotropy properties of turbulence, invariants versus eigenvalue approaches

S. BANERJEE*, †, R. KRAHL‡, F. DURST† and CH. ZENGER§

†Lehrstuhl für Stromungsmechanik, Cauerstrasse 4, Erlangen 91058, Germany
‡Lehrstuhl für Angewandte Mathematik III, Haberstr. 2, Erlangen 91058, Germany
§Lehrstuhl für Informatik mit Schwerpunkt Wissenschaftliches Rechnen,
Technical University Munich, Munich, Germany

In the literature, anisotropy-invariant maps are being proposed to represent a domain within which all realizable Reynolds stress invariants must lie. It is shown that the representation proposed by Lumley and Newman has disadvantages owing to the fact that the anisotropy invariants (*II*, *III*) are nonlinear functions of stresses. In the current work, it is proposed to use an equivalent linear representation of the anisotropy invariants in terms of eigenvalues. A barycentric map, based on the convex combination of scalar metrics dependent on eigenvalues, is proposed to provide a non-distorted visual representation of anisotropy in turbulent quantities. This barycentric map provides the possibility of viewing the normalized Reynolds stress and any anisotropic stress tensor. Additionally the barycentric map provides the possibility of quantifying the weighting for any point inside it, in terms of the limiting states (one-component, two-component, three-component). The mathematical basis for the barycentric map is derived using the spectral decomposition theorem for second-order tensors. In this way, an analytical proof is provided that all turbulence lies along the boundaries or inside the barycentric map. It is proved that the barycentric map and the anisotropy-invariant map in terms of (*II*, *III*) are one-to-one uniquely interdependent, and as a result satisfies the requirement of realizability.

Keywords: Nonlinearity; Barycentric map; Quantification of anisotropy

Nomenclature

Symbol	Description	Units	Equation
a_{ij}	Reynolds stress anisotropy tensor	—	(1)
a_{11}, a_{22}, a_{33}	diagonal components of a_{ij}	—	(1)
I, II, III	First, second and third anisotropy invariants	—	(2)
λ_1, λ_2	First and second-ordered anisotropy eigenvalues	—	(14)
$\hat{a}_{ij}$	ordered Reynolds stress anisotropy tensor	—	(17)
$\hat{a}_{1c}, \hat{a}_{2c}, \hat{a}_{3c},$	basis matrices of $\hat{a}_{ij}$	—	(24, 26, 28)
C_{1c}, C_{2c}, C_{3c}	barycentric coordinates of $\hat{a}_{ij}$	—	(32, 32, 32)
i, j	Tensor indices (double index summation)	—	
μ, ν	Tensor indices (no double index summation)	—	
δ_{ij}	Kronecker's delta	—	
$D_{1c}, D_{2c}, D_{3c},$	basis matrices of $\overline{u_i u_j}$	—	(65, 66, 67)
$D_{1cr}, D_{2cr}, D_{3cr},$	basis matrices of $\frac{\overline{u_i u_j}}{q^2}$	—	(109, 111, 113)
$C_{1cr}, C_{2cr}, C_{3cr}$	barycentric coordinates of $\frac{\overline{u_i u_j}}{q^2}$	—	(117, 118, 119)

*Corresponding author. E-mail: sankha@lstm.uni-erlangen.de, jume_sankha@yahoo.com

Journal of Turbulence
ISSN: 1468-5248 (online only)
http://www.tandf.co.uk/journals
DOI: 10.1080/14685240701506896

In this paper, all equations are written in the Cartesian coordinate system using tensor notation. An implied Einstein summation applies over a repeated subscript indices; no summation is implied for Greek indices. The SI unit system is adopted in the current work for dimensional quantities.

1. Introduction and aim of work

An important contribution to the presentation of anisotropy of turbulence has been made by Lumley [1] by the introduction of the anisotropy tensor

$$a_{ij} = \frac{\overline{u_i u_j}}{2k} - \frac{\delta_{ij}}{3}, \quad k = \frac{\overline{u_i u_i}}{2}, \tag{1}$$

and its three (principal) invariants (I, II, III):

$$I = a_{ii}, \quad II = a_{ij}a_{ji}, \quad III = a_{ij}a_{in}a_{jn} \tag{2}$$

to quantify the level of anisotropy of turbulent quantities. Lumley and Newman [2] also introduced the anisotropy-invariant map (AIM) (figure 1) taking only kinematic considerations into account as a tool to guide the development of turbulence models analytically. The AIM provides the possibility of studying the dynamics of turbulence across the functional space formed by two scalar invariants (II, III) of the anisotropy tensor. In contrast to the real space where turbulence appears to be quasi-random, three dimensional, time dependent with a

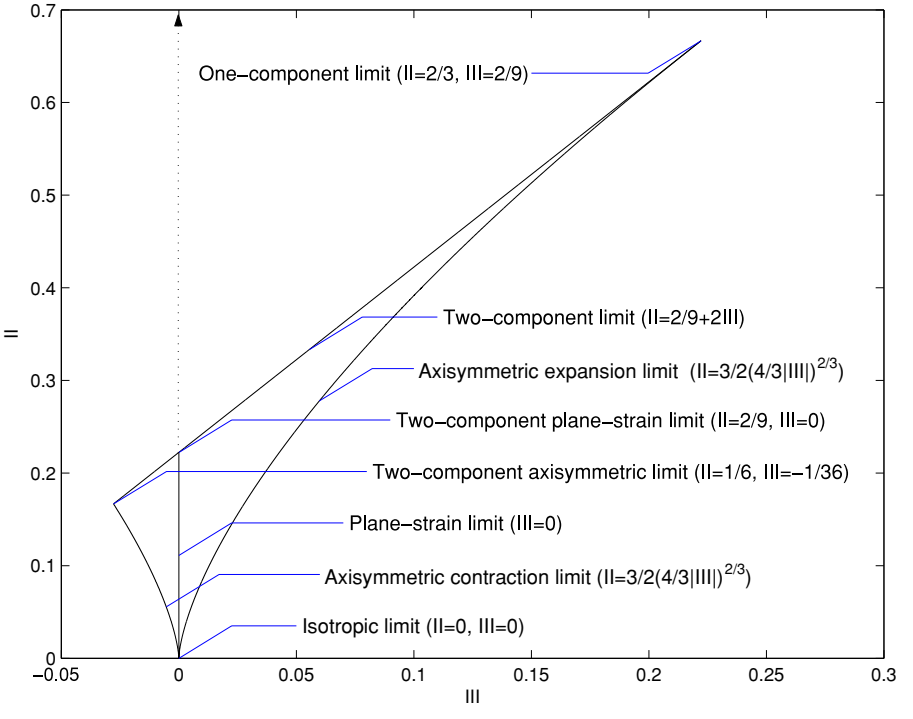

Figure 1. Anisotropy-invariant map based on (III, II).

whole hierarchy of length scales, inside the invariant space it is bounded. The AIM provides a convenient method to depict graphically any turbulence model's performance in terms of the limiting states of the map.

The anisotropy-invariant map introduced by Lumley was exploited in the modeling of turbulence by Jovanović et al. [3]. The turbulence model of Jovanović et al. based on the invariant theory and its analysis based on the AIM clearly illustrates the importance of invariant maps in the field of turbulence modeling. The AIM has been used extensively to study the trajectories of *II*, *III* invariants in various shear and wall-bounded flows to check how close they lie from the axisymmetric and two-component states [4, 5].

However Kim et al. [4] after examining the trajectories of the invariants (*II*, *III*) in fully developed channel flows in the AIM mentioned that "near the channel centerline, the flow structure indicates an approach toward isotropy." Krogstad and Torbergsen [5] mentioned that in fully developed pipe flows, the core region shows properties which permit the conclusion: "the flow structure at the centerline deviates only marginally from a state of isotropic turbulence". The presentation of turbulence properties in the AIM (figure 1) apparently permits this conclusion due to the non-linearity hidden in the definition of the variables *II* and *III*.

Moreover, it has been found that there is a confusion in the designation of the borders of the AIM. The confusion is related to whether the borders of the map describe the shape of the stress tensor or the eddies of turbulence. This controversy was noted by Choi and Lumley [6] and was apparently clarified by Krogstad et al. [7].

Recently, the eigenvalue map introduced by Lumley [1] has also been used to study trajectories of (λ_1, λ_2) of the anisotropy tensor for different flow situations [8]. The channel and the pipe flows when visualized in the eigenvalue space indicate that they are far from the states of isotropy at the centreline. Currently there is no consistent theory prevailing about which invariant maps should be preferred for visualization and modeling of anisotropy of turbulence. The current work was motivated to provide a strong equivalence between the invariant maps existing in the literature between nonlinear (*II*, *III*) and linear domains (λ_1, λ_2) and to highlight the potential advantages of the linear domains.

In the current work, the details of the usage of the barycentric map [9] in terms of eigenvalues and its potential advantages in investigating anisotropy in turbulent flows are discussed. It will be shown that the conclusions of Kim et al. [4] and Krogstad and Torbergsen [5] do not hold when the anisotropy of second-order stress tensors is viewed in the barycentric map. Scalar metrics depending on the eigenvalues of the second-order stress tensors will show that the flow properties at the channel centreline are far from isotropy. The borders of the barycentric map define the different states of the turbulent stress tensor to avoid any confusion, as noted by Choi and Lumley [6] for AIM.

Section 2 provides a summary of the basic properties of second-order stress tensors describing turbulence and shows that the linear relation between eigenvalues can be used to describe the anisotropy of second-order tensors. From linear algebra it is well known that second-order tensors are linear operators which act upon vectors to produce another vector of equal dimension. This definition motivates the representation of turbulent stress tensors in terms of linear quantities. Section 3 provides the theoretical framework for the usage of the barycentric map and computation of the barycentric coordinates within any point in the map in terms of the limiting states of the turbulent stress tensor. Section 4 provides the proof that the AIM and the barycentric map are one-to-one uniquely interdependent and discusses the important features of the barycentric formulation. Section 5 provides how the relations of axisymmetry and two-component states for the invariant map can be derived from the mathematical formulations of the barycentric map. Section 6 ends with the conclusions and the major scope of the linear barycentric map.

2. Anisotropy stress tensor and its properties

2.1 *Governing equations*

The turbulent mean flow of a viscous, incompressible fluid is governed by the Reynolds-averaged Navier–Stokes equations for mass and momentum conservation and can be written as follows:

$$\frac{\partial \overline{U_i}}{\partial x_i} = 0, \tag{3}$$

$$\frac{\partial \overline{U_j}}{\partial t} + U_i \frac{\partial \overline{U_j}}{\partial x_i} = -\frac{1}{\rho}\frac{\partial \overline{P}}{\partial x_j} + \nu \frac{\partial^2 \overline{U_j}}{\partial x_i \partial x_i} - \frac{\partial \overline{u_i u_j}}{\partial x_i} + \overline{G_j}, \tag{4}$$

where U_i is the velocity field, P is the pressure and G_j is the body forces and the overbar superscript represents the time-averaged values of the quantities. The Reynolds stress transport equations, derived with the help of the dynamic equations for the fluctuating velocity, can be expressed as

$$\underbrace{\frac{\partial \overline{u_i u_j}}{\partial t} + \overline{U}_k \frac{\partial \overline{u_i u_j}}{\partial x_k}}_{D\overline{u_i u_j}/Dt} = \underbrace{-\left(\overline{u_j u_k}\frac{\partial \overline{U}_i}{\partial x_k} + \overline{u_i u_k}\frac{\partial \overline{U_j}}{\partial x_k}\right)}_{P_{ij}} \underbrace{+\overline{\frac{p}{\rho}\left(\frac{\partial u_i}{\partial x_j} + \frac{\partial u_j}{\partial x_i}\right)}}_{\Phi_{ij}} \underbrace{-2\nu \overline{\frac{\partial u_i}{\partial x_k}\frac{\partial u_j}{\partial x_k}}}_{-\epsilon_{ij}}$$

$$\underbrace{-\frac{\partial \overline{u_i u_j u_k}}{\partial x_k}}_{D^t_{ij}} \underbrace{-\frac{1}{\rho}\left(\frac{\partial \overline{u_i p}}{\partial x_j} + \frac{\partial \overline{u_j p}}{\partial x_i}\right)}_{D^p_{ij}} \underbrace{+\nu \frac{\partial^2 \overline{u_i u_j}}{\partial x_k \partial x_k}}_{D^\nu_{ij}} \underbrace{+\overline{u_j g_i} + \overline{u_i g_j}}_{B_{ij}} \tag{5}$$

On the right-hand side of equation (5), the term P_{ij} represents the turbulence energy production, Φ_{ij} the pressure-strain correlation and ϵ_{ij} the viscous dissipation. The diffusion terms D^t_{ij}, D^p_{ij} and D^ν_{ij} represent the turbulent transport caused by the fluctuating velocity, the diffusion caused by fluctuating velocity–pressure correlation and by the viscous stresses, respectively. The last term, B_{ij}, represents a possible contribution from the body forces. This term is usually set to zero, $g_i = 0$.

In order to separate amplitude and anisotropy related behavior, it is preferable to split equation (5) into transport equations for the kinetic energy $k = \frac{1}{2}\overline{u_i u_i}$ and the Reynolds stress anisotropy tensor a_{ij}. Substituting the relationship of the anisotropy tensor (1) into transport equation (5) for the Reynolds stress tensor with the help of the kinetic energy equation, one can express the anisotropy transport system as follows:

$$\frac{\partial a_{ij}}{\partial t} + \overline{U_k}\frac{\partial a_{ij}}{\partial x_k} = \frac{1}{2k}\left(P_{ij} + \Phi_{ij} - \epsilon_{ij} + D^t_{ij} + D^p_{ij} + D^\nu_{ij} + B_{ij}\right) - \frac{1}{k}\left(a_{ij} + \frac{\delta_{ij}}{3}\right)(P - \epsilon + D^t + D^p + D^\nu + B), \tag{6}$$

where $P, \epsilon, D^t, D^p, D^\nu$ and B are the traces of $P_{ij}, \Phi_{ij}, \epsilon_{ij}, D^t_{ij}, D^p_{ij}, D^\nu_{ij}, B_{ij}$. The trace of Φ_{ij} is zero. Equation (6) for the anisotropy tensor a_{ij} together with the equation for the turbulent kinetic energy k is exactly equivalent to the transport equation (5) for the Reynolds stress tensor $\overline{u_i u_j}$. Equation (6) clearly shows that the anisotropy tensor plays a major role in turbulence modeling and its effect must be accounted for modeling the unknown correlations in equation (5).

2.2 *Properties of the reynolds stress and its anisotropy tensor*

The symmetry property of the Reynolds stress tensor $\overline{u_i u_j}$ ensures diagonalizability of its matrix. In the diagonal form, all tensor entities of $\overline{u_i u_j}$ are the matrix's eigenvalues, which are non-negative by definition. The individual components of the Reynolds stress tensor have to satisfy the physical realizability constraints (7) noted by Schumann [10]

$$\overline{u_\mu u_\mu} \geq 0, \quad \overline{u_\mu u_\mu} + \overline{u_\nu u_\nu} \geq 2|\overline{u_\mu u_\nu}|, \quad \det(\overline{u_i u_j}) \geq 0, \quad \mu, \nu = \{1, 2, 3\}. \tag{7}$$

From equation (7), it can be concluded that the Reynolds stress tensor is required to be a positive semi-definite matrix. From equation (1) and the condition of non-negativeness for the main diagonal elements in equation (7) the following relationship holds for the corresponding anisotropy tensor a_{ij}:

$$a_{\mu\mu} = \frac{\overline{u_\mu u_\mu}}{2k} - \frac{1}{3}, \quad \mu = \{1, 2, 3\}. \tag{8}$$

It can be seen that the diagonal component $a_{\mu\mu}$ of the anisotropy tensor takes its minimal value if $\overline{u_\mu u_\mu} = 0$. The maximal value corresponds to the situation when $\overline{u_\mu u_\mu} = 2k$. For the off-diagonal component $a_{\mu\nu}$ of the anisotropy tensor, one can write a similar expression

$$a_{\mu\nu} = \frac{\overline{u_\mu u_\nu}}{2k}, \quad \mu \neq \nu, \quad \mu, \nu = \{1, 2, 3\}. \tag{9}$$

Because of the positive semi-definiteness of $\overline{u_i u_j}$, the off-diagonal element $a_{\mu\nu}$ reaches its minimal value in the case when $\overline{u_\mu u_\nu} = -k$ and its maximal value if $\overline{u_\mu u_\nu} = k$. Applying these conditions to equations (8) and (9), intervals between which the anisotropy tensor components belong can be calculated:

$$-1/3 \leq a_{\mu\mu} \leq 2/3, \quad -1/2 \leq a_{\mu\nu} \leq 1/2, \quad \mu \neq \nu, \quad \mu, \nu = \{1, 2, 3\}. \tag{10}$$

2.3 *Canonical form of the anisotropy tensor*

The anisotropy tensor of Reynolds stress is also symmetric i.e, $a_{ij} = a_{ji}$. Its eigenvalues are real and the eigenvectors associated with each eigenvalue can be chosen to be mutually orthogonal. Hence the following orthogonality condition holds for the eigenvectors:

$$x_i^k x_i^l = \delta_{kl}. \tag{11}$$

Furthermore, if a tensor X_{ij} consists of the eigenvectors of a_{ij} such that the orthogonality condition (11) holds, then the tensor a_{ij} can be diagonalized by similarity transformation

$$X_{ik} a_{kl} X_{lj} = \Delta_{ij}, \tag{12}$$

where

$$\Delta_{ij} = \lambda^i \delta_{ij} \tag{13}$$

is a diagonal tensor with the eigenvalues of a_{ij} on its diagonal. The coordinate system made of the eigenvectors is termed the principal coordinate system (pcs) in which a_{ij} is diagonal.

In the current work, the following notation for the eigenvalues of the anisotropy tensor are applied:

$$\lambda_1 = \max_\mu(a_{\mu\mu}|_{\text{pcs}}), \quad \lambda_2 = \max_{\nu \neq \mu}(a_{\nu\nu}|_{\text{pcs}}), \quad \mu, \nu = \{1, 2, 3\}. \tag{14}$$

The scalar functions λ_1 and λ_2 are the two independent anisotropy eigenvalues that can be used for the characterization of the anisotropy stress tensor. From the fact that the anisotropy tensor

has a zero trace, one can represent its smallest eigenvalue by means of the above-introduced notation:

$$\lambda_3 = -\lambda_1 - \lambda_2 = \min_{\chi \neq \mu,\nu} (a_{\chi\chi}|_{\text{pcs}}). \tag{15}$$

From notation (14), the following inequality holds for the eigenvalues of a_{ij}:

$$\lambda_1 \geq \lambda_2 \geq \lambda_3. \tag{16}$$

Introducing the non-increasing order on diagonal elements of the anisotropy tensor a_{ij} (16), a_{ij} can be considered as the reordered matrix $\hat{a}_{ij}$. It can be seen that for any physically realizable Reynolds stress tensor, it is possible to construct exactly one corresponding anisotropy tensor in its canonical form (17) that can be written in terms of notation (14) as

$$\hat{a}_{ij} = \begin{pmatrix} \lambda_1 & 0 & 0 \\ 0 & \lambda_2 & 0 \\ 0 & 0 & \lambda_3 \end{pmatrix}. \tag{17}$$

2.4 *Anisotropy-invariant maps*

The anisotropy of turbulence can be characterized by the following techniques. The first representation, proposed by Lumley and Newman [2], given in figure 1, can be constructed from the following nonlinear relationships based on the two invariants of the anisotropy tensor a_{ij}, denoted by II and III:

$$II \geq \frac{3}{2}\left(\frac{4}{3}|III|\right)^{2/3}, \quad II \leq \frac{2}{9} + 2III. \tag{18}$$

The second representation suggested by Lumley [6] denoted by $\eta - \zeta$ is an alternative representation of $II - III$ denoted by $\eta - \zeta$:

$$\zeta^3 = III/2 \quad \eta^2 = -II/2. \tag{19}$$

This map is depicted in figure 2, (right). The relationships of the different boundaries of this map in terms of $\eta - \zeta$ are outlined in table 1.

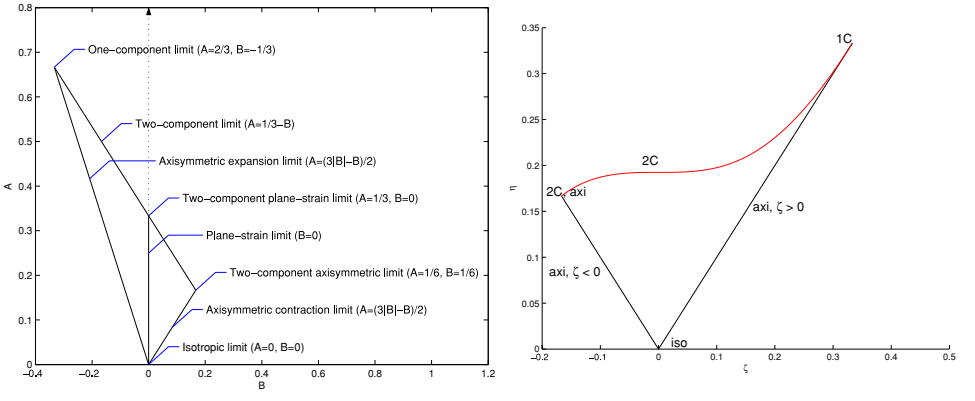

Figure 2. Anisotropy-invariant map based on two independent eigenvalues of the anisotropy tensor a_{ij}, (A, B) (left) and anisotropy invariant map based on (ζ, η) (right). The eigenvalues (A, B) correspond to λ_1, λ_2 of $\hat{a}_{ij}$.

Table 1. Characteristics of the anisotropic Reynolds stress tensor.

State of turbulence	Eigenvalues (λ_1, λ_2)	Invariants (η, ζ)
Isotropic	$\lambda_i = 0$	$\zeta = \eta = 0$
Axisymmetric expansion	$0 < \lambda_1 < \frac{1}{3}, -\frac{1}{6} < \lambda_2 = \lambda_3 < 0$	$\eta = \zeta$
Axisymmetric contraction	$-\frac{1}{3} < \lambda_1 < 0, 0 < \lambda_2 = \lambda_3 < \frac{1}{6}$	$\eta = -\zeta$
One-component limit	$\lambda_1 = \frac{2}{3}, \lambda_2 = \lambda_3 = -\frac{1}{3}$	$\zeta = -\frac{1}{6}, \eta = \frac{1}{6}$
Two-component axi-symmetric limit	$\lambda_1 = \lambda_3 = \frac{1}{6}, \lambda_2 = -\frac{1}{3}$	$\zeta = \frac{1}{3}, \eta = \frac{1}{3}$
Two-component limit	$\lambda_1 + \lambda_3 = \frac{1}{3}, \lambda_2 = -\frac{1}{3}$	$\eta = (\frac{1}{27} + 2\zeta^3)^{\frac{1}{2}}$

The third representation was originally suggested by Lumley [1], based on the eigenvalues of the anisotropy tensor, denoted by λ_1, λ_2, depicted in figure 2 (left). This representation and its relationships, as mentioned in table 1, were used in the modeling of turbulence by Terentiev [8]. The relationships of the different boundaries of this map in terms of λ_1, λ_2 are

$$\lambda_1 \geq (3|\lambda_2| - \lambda_2)/2, \quad \lambda_1 \leq 1/3 - \lambda_2. \tag{20}$$

It is easy to see that there exists a direct functional relationship between the anisotropy invariants and its corresponding eigenvalues (i.e. $II = w(\lambda_1, \lambda_2)$ and $III = q(\lambda_1, \lambda_2)$). For the transformation from the eigenvalue representation (λ_1, λ_2) to the invariants (III, II) in the principal coordinate system, one can directly use the definition for the anisotropy invariants expressed by equation (2) to obtain

$$II = 2\big(\lambda_1^2 + \lambda_1\lambda_2 + \lambda_2^2\big), \quad III = -3\lambda_1\lambda_2(\lambda_1 + \lambda_2). \tag{21}$$

Any invariant measure for a second-order tensor does not depend on the frame of reference in which the tensor is measured. Therefore, it is convenient to define different invariant measures to extract the different attributes of the tensor. Many invariant scalar measures have been introduced above, such as (II, III) and (η, ζ), which convey information about the anisotropy of $\hat{a}_{ij}$ in terms of the limiting states from the invariant maps (2).

In the present work, an alternate approach for defining invariant measures is introduced in terms of barycentric coordinates. The barycentric coordinates have the advantage of conveying the information through a barycentric map in terms of the limiting states and also locally when visualized as a 2D plot. The complete description of $\hat{a}_{ij}$ cannot be characterized by a single scalar quantity. However, many scalar quantitites can be used to convey information about the various attributes of the tensor $\hat{a}_{ij}$ such as the orientation of turbulence and the magnitude of the anisotropy.

3. States of turbulence and anisotropy invariants

3.1 *General classification of states of turbulence*

The classification of turbulence used in the present study is based on the shape of the energy ellipsoid or the componentiality of turbulence. The ellipsoid's major, medium and minor axes are along the tensor's eigenvectors, with scalings along the axes being the eigenvalues. Let $\lambda_1 \geq \lambda_2 \geq \lambda_3 \geq -\frac{1}{3}$ be the major, medium and minor eigenvalues of the $\hat{a}_{ij}$ satisfying equation (10) and let x_i be an eigenvector corresponding to λ_i.

From the spectral theorem, any second-order tensor can be written as

$$\hat{a}_{ij} = \lambda_1 x_1 x_1^T + \lambda_2 x_2 x_2^T + \lambda_3 x_3 x_3^T. \tag{22}$$

The rank, i.e. the number of non-zero eigenvalues, of the tensor $\hat{a}_{ij}$ reflects the limiting states of turbulence present in the tensor $\hat{a}_{ij}$. The limiting states of the second-order tensor can be characterized by the following states.

- *One-component* limiting state of turbulence—$(\hat{a})_{1c}$ (one eigenvalue of $\overline{u_i u_j}$ is non-zero),
- *Two-component* limiting state of turbulence—$(\hat{a})_{2c}$ (two eigenvalues of $\overline{u_i u_j}$ are non-zero),
- *Three-component* limiting state of turbulence—$(\hat{a})_{3c}$ (three eigenvalues of $\overline{u_i u_j}$ are non-zero).

In the current work, componentiality reflects the number of non-zero velocity fluctuations u_i, which matches the rank of the correlation matrix under consideration.

3.2 *Special states of turbulence of the anisotropy tensor*

One-component limiting state This case corresponds to one-rank tensor $\hat{a}_{ij}$, where $\lambda_1 > 0 > \lambda_2 \approx \lambda_3$. This is the one-component ($1c$) state of turbulence with only one component of turbulent kinetic energy. Turbulence in an area of this type is only along one direction, the direction of the eigenvector corresponding to the non-zero eigenvalue

$$\hat{a}_{ij} \cong \lambda_1 x_1 x_1^T \cong \lambda_1 \hat{a}_{1c}. \tag{23}$$

The basis matrix for the limiting state is given by

$$\hat{a}_{1c} = \begin{pmatrix} 2/3 & 0 & 0 \\ 0 & -1/3 & 0 \\ 0 & 0 & -1/3 \end{pmatrix}. \tag{24}$$

Two-component limiting state This case corresponds to two-rank tensor $\hat{a}_{ij}$, where the $\lambda_1 \approx \lambda_2 > 0 > \lambda_3$. This is the two-component ($2c$) isotropic state of turbulence, where the one component of turbulent kinetic energy vanishes with the remaining two being equal. Turbulence in an area of this type is restricted to planes, the plane spanned by the two eigenvectors corresponding to non-zero eigenvalues

$$\hat{a}_{ij} \cong \lambda_1 \left(x_1 x_1^T + x_2 x_2^T \right) \cong \lambda_1 \hat{a}_{2c}. \tag{25}$$

The basis matrix for the limiting state is given by

$$\hat{a}_{2c} = \begin{pmatrix} 1/6 & 0 & 0 \\ 0 & 1/6 & 0 \\ 0 & 0 & -1/3 \end{pmatrix}. \tag{26}$$

Three-component limiting state This case corresponds to three-rank tensor $\hat{a}_{ij}$, where $\lambda_1 = \lambda_2 = \lambda_3$. This is the three-component ($3c$) isotropic state of turbulence. Turbulence in an area of this type is restricted to a sphere, the axes of the sphere are spanned by the eigenvectors corresponding to non-zero eigenvalues

$$\hat{a}_{ij} \cong \lambda_1 \left(x_1 x_1^T + x_2 x_2^T + x_3 x_3^T \right) \cong \lambda_1 \hat{a}_{3c}. \tag{27}$$

The basis matrix for this limiting state is given by

$$\hat{a}_{3c} = \begin{pmatrix} 0 & 0 & 0 \\ 0 & 0 & 0 \\ 0 & 0 & 0 \end{pmatrix}. \tag{28}$$

$$\hat{a}_{ij} = C_{1c}\hat{a}_{1c} + C_{2c}\hat{a}_{2c} + C_{3c}\hat{a}_{3c} \tag{29}$$

$$C_{1c} \geq 0, C_{2c} \geq 0, C_{3c} \geq 0, \tag{30}$$

where $\{C_{1c}, C_{2c}, C_{3c}\}$ are the coordinates of the anisotropy tensor $\hat{a}_{ij}$ in the tensor basis $\{\hat{a}_{1c}, \hat{a}_{2c}, \hat{a}_{3c}\}$. As described above, the relationships between the eigenvalues of the anisotropy tensor can be used for the classification of the $\hat{a}_{ij}$ by using the coordinates of the tensor in the new basis $\hat{a}_{1c}, \hat{a}_{2c}$ and $\hat{a}_{3c}$ to measure how close $\hat{a}_{ij}$ is from the generic cases of one-component, two-component and three-component limiting states. To obtain a measure of anisotropy from the anisotropy tensor $\hat{a}_{ij}$, metrics of three different kinds of anisotropy are provided.

The normalizing coefficient is chosen in a manner such that

$$C_{1c} + C_{2c} + C_{3c} = 1, \tag{31}$$

where C_{1c} is a linear measure of anisotropy and C_{2c} is the planar measure of anisotropy. The normalization is done in such a way that all metrics $\{C_{1c}, C_{2c}, C_{3c}\}$ lie in the range [0, 1]. It has to be noted that $\hat{a}_{3c}$ is a null matrix which can make equation (29) non-unique but the restriction on C_{3c} using (31) makes it unique.

In general, any anisotropy tensor $\hat{a}_{ij}$ can be expressed as a convex combination (29) of the limiting states (one-component, two-component, three-component) by setting

$$C_{1c} = \lambda_1 - \lambda_2 \tag{32}$$

$$C_{2c} = 2(\lambda_2 - \lambda_3) \tag{33}$$

$$C_{3c} = 3\lambda_3 + 1. \tag{34}$$

An anisotropy measure describing the deviation from isotropy is achieved as

$$C_{ani} = C_{1c} + C_{2c} \tag{35}$$

$$C_{ani} = 1 - C_{3c} \tag{36}$$

$$C_{ani} = -3\lambda_3. \tag{37}$$

Taking the above formulation into account, a barycentric map [9] can be used to characterize turbulence where the three limiting states of turbulence (one-component, two-component, three-component) represent the three vertices of the map. In the current barycentric map, at each vertex one of the metrics $\{C_{1c}, C_{2c}, C_{3c}\}$ has coefficient 1 and then it decreases to zero for the line opposite to the vertex. A value of 1 for any of the metrics corresponds to the respective limiting states and a value of 0 means that the respective limiting state does not have any contribution to the current state. Any point inside the map has local barycentric coordinates $\{C_{1c}, C_{2c}, C_{3c}\}$ which helps to know directly the weighting of the three limiting states of turbulence at that point and so quantification of the anisotropy is possible. The mathematical formulation which can be used for the normalized Reynolds stress tensor is given in appendix B.

3.3 *Plotting of the map*

The barycentric map can be used as a tool to visualize the nature of anisotropy in $\hat{a}_{ij}$ for different types of turbulent flows. For plotting the barycentric map, we identify the basis matrices $\hat{a}_{1c}$, $\hat{a}_{2c}$ and $\hat{a}_{3c}$ of equation (29) as the three vertices of the triangle. The vertices of the map can be identified as three points (x_{1c}, y_{1c}), (x_{2c}, y_{2c}) and (x_{3c}, y_{3c}) in the Euclidean space representing the three limiting states. To plot a point, we have to take a convex combination of the limiting

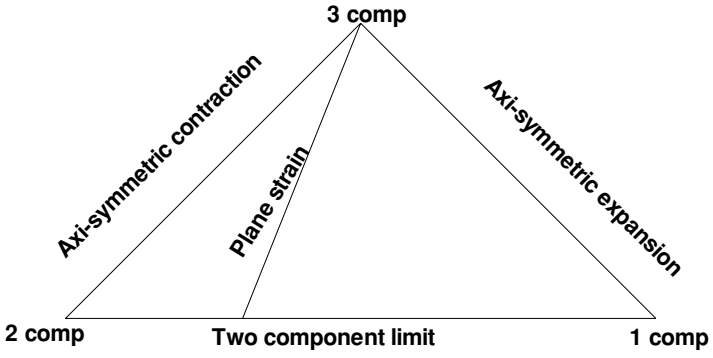

Figure 3. Barycentric map based on scalar metrics which are functions of eigenvalues of the second-order stress tensor describing turbulence. The isotropic point has a metric $C_{3c} = 1$, the two-component point has $C_{2c} = 1$ and the one -component point has $C_{1c} = 1$.

states (32)–(34) using equation (29):

$$x_{\text{new}} = C_{1c}x_{1c} + C_{2c}x_{2c} + C_{3c}x_{3c} \tag{38}$$

$$y_{\text{new}} = C_{1c}y_{1c} + C_{2c}y_{2c} + C_{3c}y_{3c}. \tag{39}$$

All flows can be plotted in the barycentric map figure 3 using relations (38), (39) to visualize the nature of anisotropy in $\hat{a}_{ij}$. An important point which needs to be noted in the construction of the barycentric map is that all the limiting states (one-component, two-component, three-component) are joined by lines. The proof that these limiting states can be joined by lines is given in appendix A. Another important feature of the barycentric map is that it can be constructed by taking three arbitrary basis points such as (x_{1c}, y_{1c}), (x_{2c}, y_{2c}) and (x_{3c}, y_{3c}) so one can choose the basis of figure 2, (left) to obtain the eigenvalue map. The barycentric map is depicted in the form of an equilateral triangle as all the metrics (32)–(34) scale from [0, 1] and an equilateral triangle does not introduce any visual bias of the limiting states (one-component, two-component, three-component).

3.4 *Computation of the barycentric coordinates*

The scalar metrics C_{1c}, C_{2c} and C_{3c} are computed from relations (32)–(34). Figure 4 shows the $\hat{a}_{ij}$ distribution for a fully developed plane turbulent channel flow at $Re_\tau = 180$. Figure 4 clearly illustrates that the mathematical requirement of axisymmetry $\hat{a}_{22} = \hat{a}_{33}$ is not satisfied, but when it is viewed in the AIM figure 5 (left) it gives a visual impression of axisymmetry. The barycentric map figure 5 (right) is much more consistent in preserving this physical information, and it shows that the fully developed plane turbulent channel flow for $Re_\tau = 180$ is far from axisymmetry. In figure 5 (right) it can be observed that the barycentric map offers a visual advantage in depicting that the channel flow is far from isotropy at the channel centerline. The weighting of the limiting states for plane channel flow data of Kim et al. [11] was computed, and it was found that the isotropic metric C_{3c} is 0.9 and not 1 to indicate full isotropy of the flow at the channel centerline. Table 2 gives a clear mathematical justification that the channel flows are not isotropic at the centerline as claimed by Kim et al. [4]. The nonlinearity in (II, III) makes the flow tend toward isotropy visually when viewed in the AIM (figure 5, left). Similar conclusions can be drawn about pipe flows when they are viewed in the barycentric map.

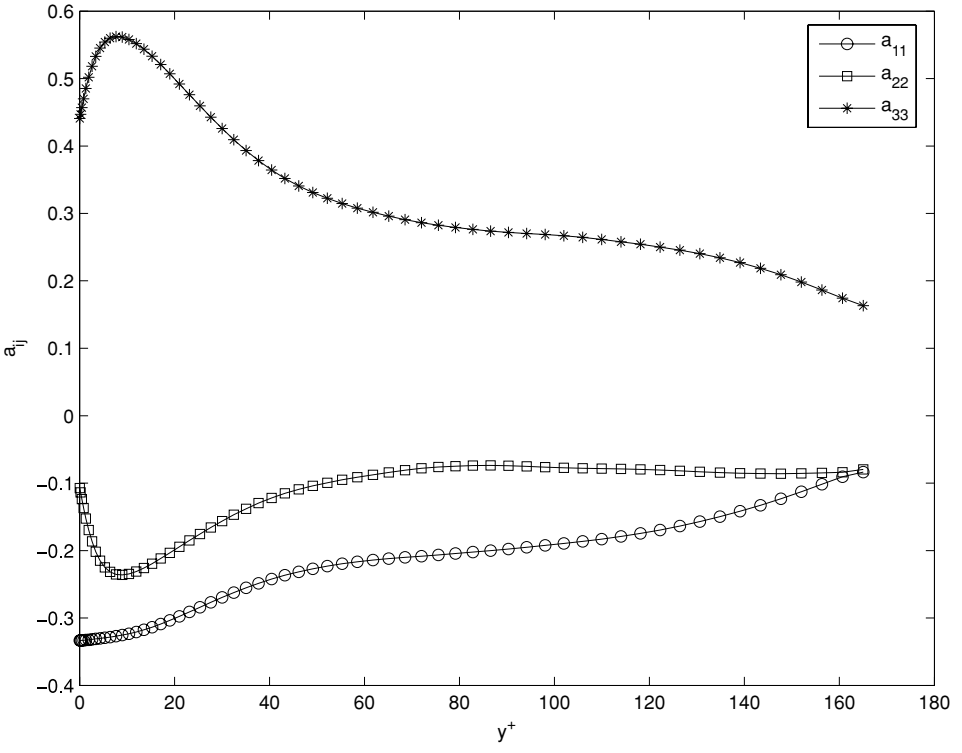

Figure 4. The $\hat{a}_{ij}$ distribution from data of direct numerical simulation of fully developed plane turbulent channel flow for $Re_\tau = 180$ by Kim et al. [11]. The $\hat{a}_{33}$ stresses are 200% more than the $\hat{a}_{22}$ stresses near the wall of the channel and meet the axisymmetry criterion only at the channel centerline.

From figure 6, (left), it is important to observe that when the point P, when projected to any one side of the barycentric map, say for instance, the two-component side, the distance from the two-component vertex to the line $C_{1c} = 0.5$ intercepts is the quantitative value of C_{1c}; similarly the distance from the one-component vertex to the line $C_{2c} = 0.25$ intercepts

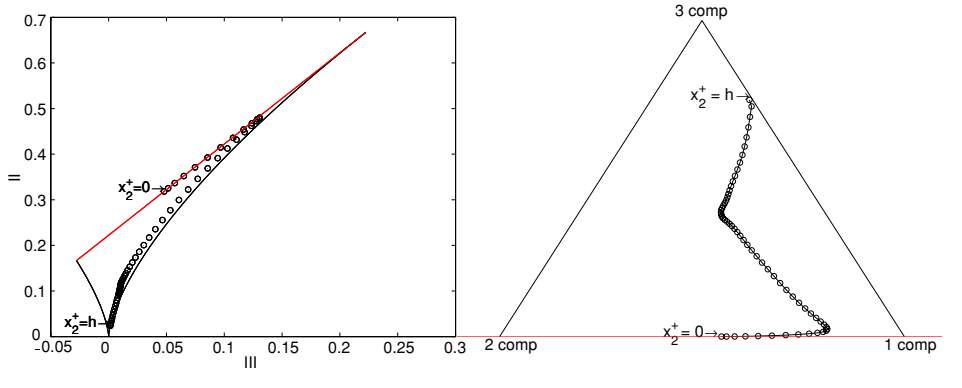

Figure 5. Invariant characteristics of the anisotropy tensors for the Reynolds stress [○] - $\overline{u_i u_j}$ on the anisotropy-invariant map (III, II) (left) and scalar metrics (C_{1c}, C_{2c}) based on the eigenvalues of anisotropy tensor for the Reynolds stress on the barycentric map (right). Data were extracted from a direct numerical simulation of fully developed plane turbulent channel flow for $Re_\tau = 180$ by Kim et al. [11].

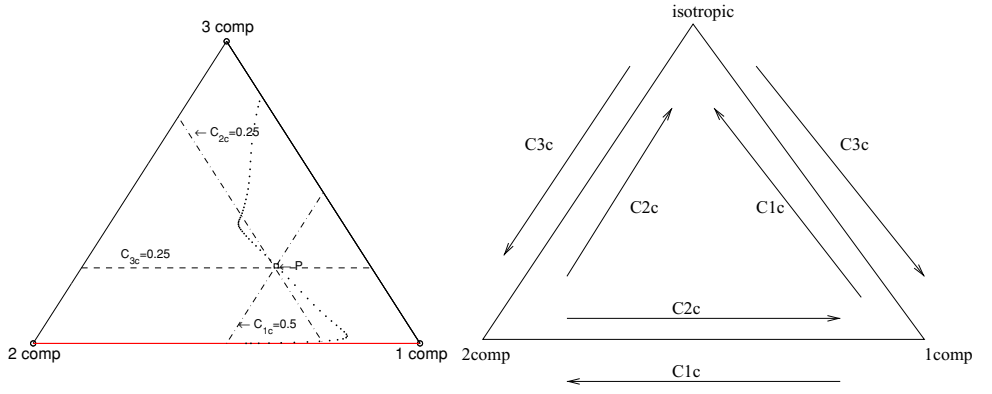

Figure 6. Calculation of the weighting of a point P from data extracted from a direct numerical simulation of fully developed plane turbulent channel flow for $Re_\tau = 180$ on the barycentric map (left) and the axis of the metrics C_{1c}, C_{2c} and C_{3c} on the barycentric map (right). The isotropic point corresponds to three-component.

is the value of C_{2c}. The value of C_{3c} can be obtained from equation (31) and in the map it is the distance between the line joining the one- and two-component states and the line where $C_{3c} = 0.25$ along the sides of the barycentric map. The manner in which the barycentric coordinates scale in the barycentric map is shown in figure (6), (right). The center of the barycentric map corresponds to the point P where

$$C_{1c} = \frac{1}{3}, \quad C_{2c} = \frac{1}{3}, \quad C_{3c} = \frac{1}{3} \tag{40}$$

The center of the barycentric map when mapped back on to the invariant map (AIM) gives a point very close to the axi-symmetric expansion curve which can be verified by inserting the barycentric coordinates (40) into (43). This fact can be visually noticed in the invariant map (AIM), figure (7) (left) and in the barycentric map figure (7) (right). This is a mathematical justification about the fact, why channel flows which are far away from the axi-symmetric limiting states in the barycentric map figure 5 (right) and are so near to the axi-symmetric limiting states in the AIM figure 5 (left).

4. Mapping between the barycentric and the invariant map

In this section we show that there is a bijection between the barycentric map and the invariant map. The domain of the invariant map (AIM) is bounded by the line $II = \frac{3}{2}(\frac{4}{3}III)^{\frac{2}{3}}$ from below and by $II = 2III + \frac{2}{9}$ from above. In other words, a point (III, II) lies inside the invariant map if and only if

$$\frac{3}{2}\left(\frac{4}{3}III\right)^{\frac{2}{3}} \leq II \leq 2III + \frac{2}{9}. \tag{41}$$

Table 2. Weightings of the point P.

Points	C_{1c}	C_{2c}	C_{3c}
P	0.5	0.25	0.25
$x_2^+ = h$	0.1	0.0	0.9
$x_2^+ = 0$	0.55	0.45	0.0

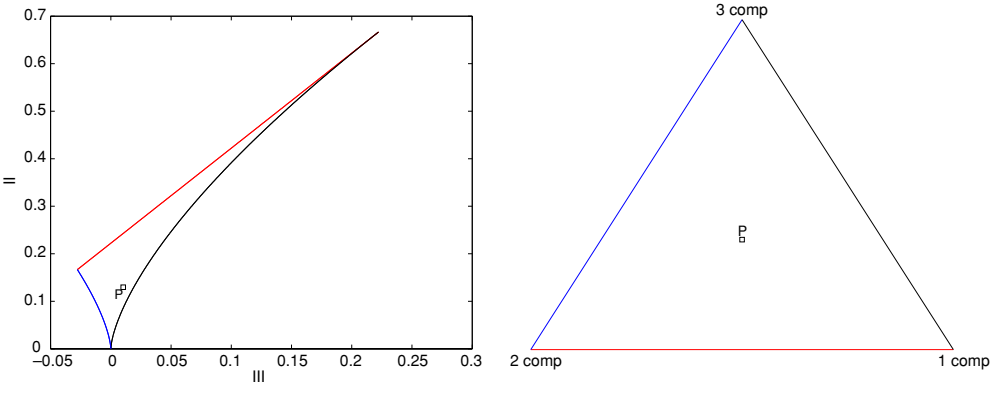

Figure 7. The centrepoint P of the barycentric map (right) projected onto the invariant map (left). The point P lies closer to the axisymmetric states in the invariant map.

Let the barycentric coordinates C_{1c}, C_{2c} and C_{3c} of the barycentric map be given, and from definitions (32)–(34) we obtain

$$\begin{aligned}\lambda_1 &= C_{1c} + \frac{C_{2c}}{2} + \frac{C_{3c}}{3} - \frac{1}{3},\\ \lambda_2 &= \frac{C_{2c}}{2} + \frac{C_{3c}}{3} - \frac{1}{3},\\ \lambda_3 &= \frac{C_{3c}}{3} - \frac{1}{3}.\end{aligned} \tag{42}$$

Substituting $C_{3c} = 1 - C_{1c} - C_{2c}$, we deduce

$$\begin{aligned}II &= \left(\frac{2}{3}C_{1c} + \frac{1}{6}C_{2c}\right)^2 + \left(-\frac{1}{3}C_{1c} + \frac{1}{6}C_{2c}\right)^2 + \left(-\frac{1}{3}C_{1c} - \frac{1}{3}C_{2c}\right)^2\\ &= \frac{2}{3}C_{1c}^2 + \frac{1}{3}C_{1c}C_{2c} + \frac{1}{6}C_{2c}^2,\\ III &= \left(\frac{2}{3}C_{1c} + \frac{1}{6}C_{2c}\right)^3 + \left(-\frac{1}{3}C_{1c} + \frac{1}{6}C_{2c}\right)^3 + \left(-\frac{1}{3}C_{1c} - \frac{1}{3}C_{2c}\right)^3\\ &= \frac{2}{9}C_{1c}^3 + \frac{1}{6}C_{1c}^2C_{2c} - \frac{1}{12}C_{1c}C_{2c}^2 - \frac{1}{36}C_{2c}^3.\end{aligned} \tag{43}$$

This means that we can express II and III in terms of the barycentric coordinates C_{1c}, C_{2c} and C_{3c} and this defines a mapping $(III, II) = \Phi(C_{1c}, C_{2c}, C_{3c})$ from the barycentric map into the II–III plane of the invariant map.

4.1 *Range of the mapping*

In order to show that the range of Φ lies within the bounds of the invariant map (41), let C_{1c}, C_{2c} and C_{3c} be the barycentric coordinates of some point in the barycentric map, using equation (43), we deduce

$$\begin{aligned}\left(\frac{2}{3}II\right)^3 - \left(\frac{4}{3}III\right)^2 &= \frac{4}{27}C_{1c}^4C_{2c}^2 + \frac{4}{27}C_{1c}^3C_{2c}^3 + \frac{1}{27}C_{1c}^2C_{2c}^4\\ &\geq 0\end{aligned} \tag{44}$$

and

$$
\begin{aligned}
&2\,III + \frac{2}{9} - II \\
&= \frac{4}{9}C_{1c}^3 + \frac{1}{3}C_{1c}^2 C_{2c} - \frac{1}{6}C_{1c}C_{2c}^2 - \frac{1}{18}C_{2c}^3 - \frac{2}{3}C_{1c}^2 - \frac{1}{3}C_{1c}c_{2C} - \frac{1}{6}C_{2c}^2 + \frac{2}{9} \\
&= C_{3c}C_{2c}\left(C_{1c} + \frac{1}{2}C_{2c}\right) + \frac{2}{9}C_{3c}^2(1 + 2C_{1c} + 2C_{2c}) \\
&\geq 0. \qquad (45)
\end{aligned}
$$

Therefore, we have $\frac{3}{2}(\frac{4}{3}III)^{\frac{2}{3}} \leq II \leq 2\,III + \frac{2}{9}$, and thus the point (III, II) lies inside the domain of the invariant map (AIM).

4.2 *Mapping from the invariant coordinates to the barycentric coordinates*

Let (III, II) be a point in the invariant map, fulfilling relation (41). We have to show that there are barycentric coordinates C_{1c}, C_{2c} and C_{3c} fulfilling the relation $(III, II) = \Phi(C_{1c}, C_{2c}, C_{3c})$.

Consider the cubic function which defines the relation between (III, II) and (λ_1, λ_2):

$$f(x) = 3\,x^3 - \frac{3}{2}\,I\,I\,x - III. \qquad (46)$$

The critical points of f are at $x_{c1} = -\sqrt{\frac{1}{6}\,II}$ and $x_{c2} = +\sqrt{\frac{1}{6}\,II}$ with $f(x_{c1}) = +\sqrt{\frac{1}{6}\,I\,I^3} - III$ and $f(x_{c2}) = -\sqrt{\frac{1}{6}\,II^3} - III$. From relation (41), it follows that $f(x_{c1}) \geq 0$ and $f(x_{c2}) \leq 0$. Therefore, f must have exactly one root β with

$$-\sqrt{\frac{1}{6}\,II} \leq \beta \leq +\sqrt{\frac{1}{6}\,II} \qquad (47)$$

and from equation (46)

$$3\,\beta^3 - \frac{3}{2}\,II\,\beta = III. \qquad (48)$$

Choosing

$$
\begin{aligned}
\alpha &= +\sqrt{\frac{1}{2}\,II - \frac{3}{4}\,\beta^2} - \frac{1}{2}\,\beta, \\
\gamma &= -(\alpha + \beta). \qquad (49)
\end{aligned}
$$

then from relation (47) it follows that

$$\frac{1}{2}\,II - \frac{3}{4}\,\beta^2 \geq \frac{3}{8}\,II \geq 0 \qquad (50)$$

Hence α is real and $\beta \leq +\sqrt{\frac{1}{6}\,II} \leq \alpha$. In a similar way, it can be proved that $\gamma \leq -\sqrt{\frac{1}{6}\,II} \leq \beta$. The estimate $-\frac{1}{3} \leq \gamma$ can be derived from $II \leq 2\,III + \frac{2}{9}$.

4.3 *Uniqueness in the mapping from the barycentric map to the invariant map*

Let (c_{1c}, c_{2c}, c_{3c}) and $(\tilde{c}_{1c}, \tilde{c}_{2c}, \tilde{c}_{3c})$ be the barycentric coordinates of two points in the barycentric map, fulfilling relations (30) and (31) respectively, that are mapped to the same point (III, II) in the anisotropy map by Φ. That is, we have

$$(III, II) = \Phi(c_{1c}, c_{2c}, c_{3c}) = \Phi(\tilde{c}_{1c}, \tilde{c}_{2c}, \tilde{c}_{3c}) \tag{51}$$

with Φ as defined by 43. In order to prove the injectivity of Φ, we have to show that $(c_{1c}, c_{2c}, c_{3c}) = (\tilde{c}_{1c}, \tilde{c}_{2c}, \tilde{c}_{3c})$.
Let

$$\begin{aligned}
\alpha &= \frac{2}{3}\,c_{1c} + \frac{1}{6}\,c_{2c}, \quad \tilde{\alpha} = \frac{2}{3}\,\tilde{c}_{1c} + \frac{1}{6}\,\tilde{c}_{2c},\\
\beta &= -\frac{1}{3}\,c_{1c} + \frac{1}{6}\,c_{2c}, \quad \tilde{\beta} = -\frac{1}{3}\,\tilde{c}_{1c} + \frac{1}{6}\,\tilde{c}_{2c},\\
\gamma &= -\frac{1}{3}\,c_{1c} - \frac{1}{3}\,c_{2c}, \quad \tilde{\gamma} = -\frac{1}{3}\,\tilde{c}_{1c} - \frac{1}{3}\,\tilde{c}_{2c}.
\end{aligned} \tag{52}$$

Note that we have $\alpha+\beta+\gamma = 0, \tilde{\alpha}+\tilde{\beta}+\tilde{\gamma} = 0$, and by equation 30 $\alpha \geq \beta \geq \gamma, \tilde{\alpha} \geq \tilde{\beta} \geq \tilde{\gamma}$. Using this definition, we can write equation 51 as

$$II = \alpha^2 + \beta^2 + (-\alpha - \beta)^2 = \tilde{\alpha}^2 + \tilde{\beta}^2 + (-\tilde{\alpha} - \tilde{\beta})^2, \tag{53a}$$

$$III = \alpha^3 + \beta^3 + (-\alpha - \beta)^3 = \tilde{\alpha}^3 + \tilde{\beta}^3 + (-\tilde{\alpha} - \tilde{\beta})^3. \tag{53b}$$

Note that

$$\frac{1}{6}\,II - \beta^2 = \frac{1}{6}\,c_{1c}\,c_{2c} \geq 0 \tag{54}$$

and thus $\beta \in [-\sqrt{\frac{1}{6}\,II}, +\sqrt{\frac{1}{6}\,II}]$. Similarly, $\tilde{\beta} \in [-\sqrt{\frac{1}{6}\,II}, +\sqrt{\frac{1}{6}\,II}]$.
Combining equations (53*a*) and (53*b*) we obtain

$$\begin{aligned}
&\frac{3}{2}\,\beta\,II + III = 3\beta^3 \quad \text{and}\\
&\frac{3}{2}\,\tilde{\beta}\,II + III = 3\tilde{\beta}^3.
\end{aligned} \tag{55}$$

In other words, β and $\tilde{\beta}$ are both roots of $f(x) = 3\,x^3 - \frac{3}{2}\,II\,x - III$. We already checked above that f has only one root in the range $[-\sqrt{\frac{1}{6}\,II}, +\sqrt{\frac{1}{6}\,II}]$ and therefore we get

$$\beta = \tilde{\beta}. \tag{56}$$

From equation (53*a*), we obtain

$$\alpha = \pm\sqrt{\frac{1}{2}\,II - \frac{3}{4}\,\beta^2} - \frac{1}{2}\,\beta. \tag{57}$$

Insertion into $\gamma = -\alpha - \beta$ yields

$$\gamma = \mp\sqrt{\frac{1}{2}\,II - \frac{3}{4}\,\beta^2} - \frac{1}{2}\,\beta. \tag{58}$$

Observing that $\alpha \geq \gamma$ and using the same arguments on $\tilde{\alpha}$ and $\tilde{\gamma}$, we conclude that

$$\alpha = +\sqrt{\frac{1}{2}II - \frac{3}{4}\beta^2} - \frac{1}{2}\beta = +\sqrt{\frac{1}{2}II - \frac{3}{4}\tilde{\beta}^2} - \frac{1}{2}\tilde{\beta} = \tilde{\alpha} \tag{59}$$

and finally

$$\gamma = -\alpha - \beta = -\tilde{\alpha} - \tilde{\beta} = \tilde{\gamma}. \tag{60}$$

Now we can deduce from equation (52) that

$$\begin{aligned} c_{1c} &= \alpha - \beta = \tilde{\alpha} - \tilde{\beta} = \tilde{c}_{1c} \\ c_{2c} &= 2(\beta - \gamma) = 2(\tilde{\beta} - \tilde{\gamma}) = \tilde{c}_{2c} \\ c_{3c} &= 3\gamma + 1 = 3\tilde{\gamma} + 1 = \tilde{c}_{3c}. \end{aligned} \tag{61}$$

This completes the proof of the injectivity of Φ.

4.4 *Important features of the barycentric coordinates*

Figure 8 describes an easy way of obtaining the interpolation between any two points on the AIM exactly. Taking a point having coordinates (*II*, *III*) in the AIM we can find the eigenvalues corresonding to it by using equation (46). Once the eigenvalues are known, the barycentric metrics (32)–(34) can be computed. So if the linear interrelationships between unknown second-order tensors are desired, as in Jovanović et al. [12] then the two points can be joined by a line in the linear domain of barycentric map and then converted back to invariants using equation (43). This provides a consistent and sound mathematical interpolation schemes between two points in the invariant map.

Figure 9 plots the barycentric metrics C_{1c}, C_{2c} and C_{3c} on the y-axis and y^+ on the x-axis from direct numerical simulation data of fully developed plane turbulent channel flow for $Re_\tau = 180$ [11]. This 2D plot provides quantitative information about how $\hat{a}_{ij}$ behaves in terms of the limiting states (one-component, two-component and three-component) locally. Figure 9 also provides the information that any point inside the barycentric map figure 3 bears the same area ratio (i.e. take any point in the barycentric map or the eigenvalue map of Lumley and join that point with the limiting states of the map, the ratio of the areas of the three sub-triangles to the total area of the triangle is referred to as the area ratio) as in the Lumley triangle figure 2 (left). Figure 9 provides the possibility of studying the dominance of the C_{1c}

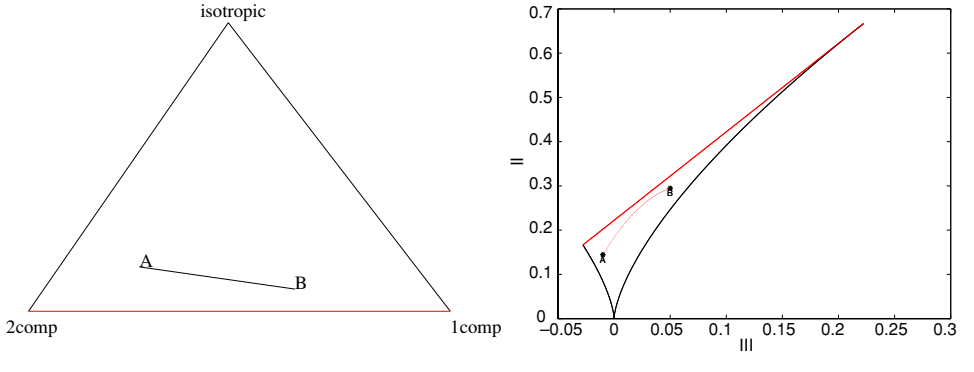

Figure 8. Linear interpolation between two points inside the barycentric map projected onto the invariant map. The isotropic point corresponds to three-component.

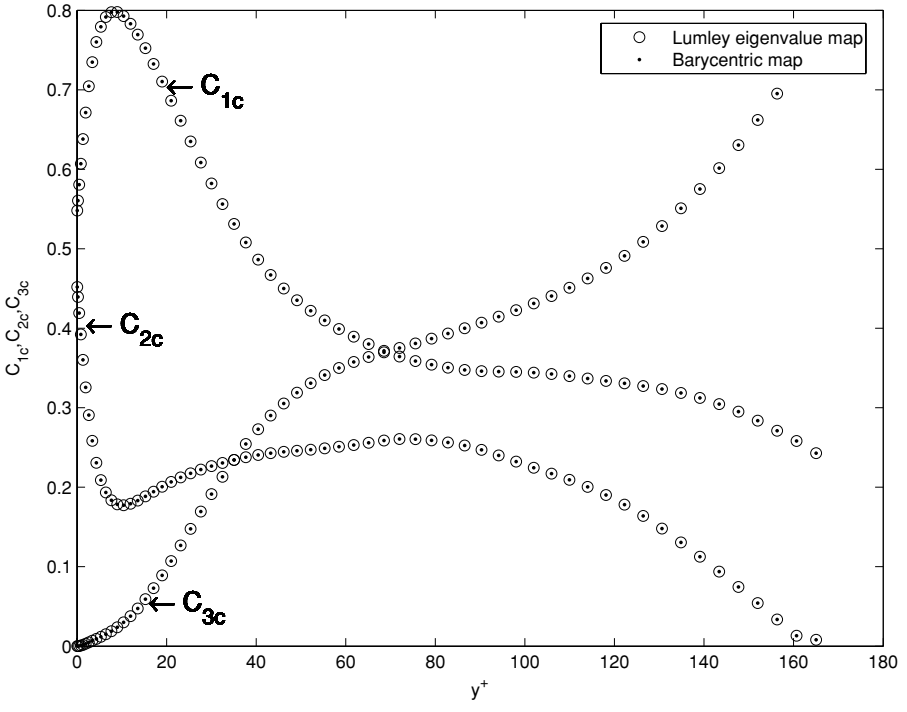

Figure 9. At any point in the flow exact weighting can be found in terms of the limiting states. Data were extracted from a direct numerical simulation of fully developed plane turbulent channel flow for $Re_\tau = 180$ by Kim et al. [11].

and C_{2c} in the near-wall region and the dominance of C_{3c} over C_{2c} and C_{1c} at the centerline for $\hat{a}_{ij}$. It is interesting to observe that at the channel centerline the C_{1c} metric goes to zero.

It is also interesting to note that the return to isotropy experiments for plane strain of Choi [6] when viewed in the barycentric map figure (12) (left) they show no tendency to get aligned with the axisymmetric expansion state as claimed by Choi et al. [6]. This fact is further substantiated by investigating the scalar metrics C_{1c} and C_{2c} in the 2D plot figure 12 (right) where $C_{2c} \neq 0$ signifies that return to isotropy from plane strain experiments cannot be claimed have the same behavior like axi-symmetric expansion ($C_{1c} = 0$).

Figure 10 shows how the barycentric map captures the channel flow in three-dimensional space [11]. This projection of a three-dimensional flow is possible only in linear domain and not in a nonlinear domain such as the AIM. From figure 11 it can be observed that when a uniform distribution of randomly generated anisotropic stress tensors $\hat{a}_{ij}$ are plotted in the barycentric map and mapped back to the invariant map the distribution is quite different. This fact illustrates that conclusion of physical facts (i.e nearness to axisymmetric and two-component limits) for any turbulent flow should not be made based on visual observation. It has to be noted that invariant maps based on (II, III), (λ_1, λ_2) and (C_{1c}, C_{2c}) are not sensitive to the individual energy components of the anisotropic stress tensors, as it can be shown that two totally different individual energy component anisotropic stress tensors having trace zero will be mapped to the same point in the above anisotropy invariant maps. The information which is preserved between two anisotropic stress tensors mapped to two different points in the anisotropy invariant maps is their distance from the limiting states (one-component, two-component and three-component).

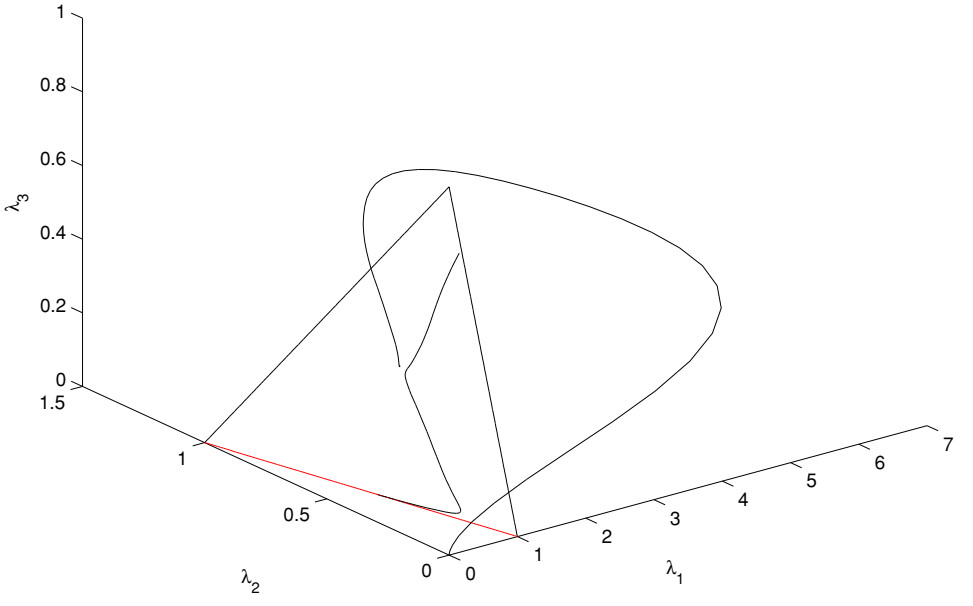

Figure 10. Scalar metrics based on the eigenvalues of anisotropy tensor $\hat{a}_{ij}$ projected onto the barycentric map. Data were extracted from a direct numerical simulation of fully developed plane turbulent channel flow for $Re_\tau = 180$ by Kim et al. [11].

5. Relationship between invariants and barycentric coordinates

In this section, we prove that the axisymmetry and the two-dimensional relationships of the AIM can be derived from equations (29). The anisotropy tensor $\hat{a}_{ij}$ for the limiting states of turbulence are described in the following ways:

$$\hat{a}_{1c} = \frac{D_{1c}}{\text{trace}D_{1c}} - \frac{1}{3} \tag{62}$$

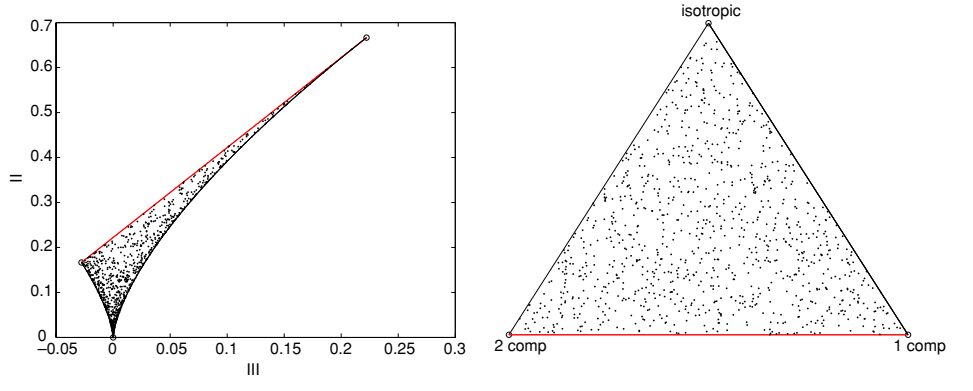

Figure 11. Randomly generated anisotropic tensors $\hat{a}_{ij}$ which are uniformly distributed in the linear barycentric space (right) mapped back to the nonlinear space (III, II) (left). The nonlinearity in II, III of the invariant space concentrates the points near isotropy. The isotropic point corresponds to three-component.

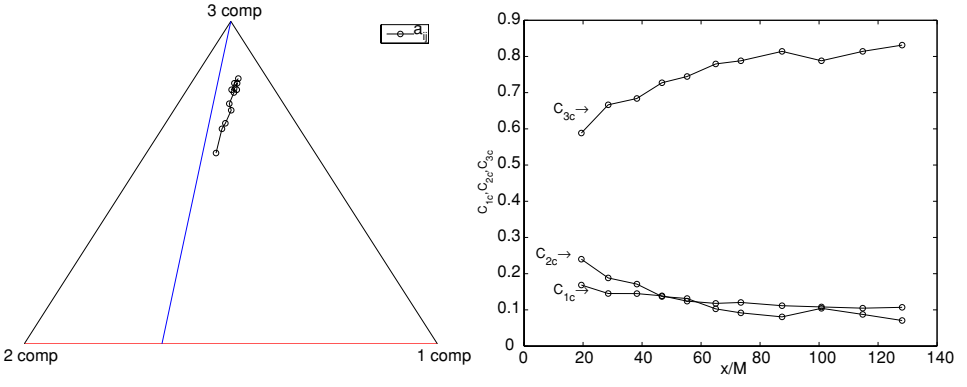

Figure 12. Scalar metrics C_{1c}, C_{2c} and C_{3c} of the $\hat{a}_{ij}$ for plane strain (case—plane strain [6]) plotted inside the barycentric map (left) and as x–y plot (right).

$$\hat{a}_{2c} = \frac{D_{2c}}{\text{trace}D_{2c}} - \frac{1}{3} \tag{63}$$

$$\hat{a}_{3c} = \frac{D_{3c}}{\text{trace}D_{3c}} - \frac{1}{3} \tag{64}$$

$$D_{1c} = \begin{pmatrix} 1 & 0 & 0 \\ 0 & 0 & 0 \\ 0 & 0 & 0 \end{pmatrix} \tag{65}$$

$$D_{2c} = \begin{pmatrix} 1 & 0 & 0 \\ 0 & 1 & 0 \\ 0 & 0 & 0 \end{pmatrix} \tag{66}$$

$$D_{3c} = \begin{pmatrix} 1 & 0 & 0 \\ 0 & 1 & 0 \\ 0 & 0 & 1 \end{pmatrix}. \tag{67}$$

For the *one-component limit* the invariants can be found as

$$II = \left(\frac{2}{3}\right)^2 + \left(-\frac{1}{3}\right)^2 + \left(-\frac{1}{3}\right)^2 \tag{68}$$

$$III = \left(\frac{2}{3}\right)^3 + \left(-\frac{1}{3}\right)^3 + \left(-\frac{1}{3}\right)^3. \tag{69}$$

For the *two-component limit* the invariants can be found as

$$II = \left(\frac{1}{6}\right)^2 + \left(\frac{1}{6}\right)^2 + \left(-\frac{1}{3}\right)^2 \tag{70}$$

$$III = \left(\frac{1}{6}\right)^3 + \left(\frac{1}{6}\right)^3 + \left(-\frac{1}{3}\right)^3. \tag{71}$$

For the *isotropic limit* the invariants can be found as

$$I\,I = 0 \tag{72}$$

$$III = 0. \tag{73}$$

The matrix for the axisymmetric expansion boundary from equation (29) and taking $C_{2c} = 0$ is given as

$$\hat{a}_{1c-3c} = C_{1c}\begin{pmatrix} 2/3 & 0 & 0 \\ 0 & -1/3 & 0 \\ 0 & 0 & -1/3 \end{pmatrix} + C_{3c}\begin{pmatrix} 0 & 0 & 0 \\ 0 & 0 & 0 \\ 0 & 0 & 0 \end{pmatrix} \tag{74}$$

Using relation (31), let us take $C_{1c} = \kappa$ and $C_{3c} = 1-\kappa$, therefore the invariants can be found as

$$II = \left(\frac{2}{3}\kappa\right)^2 + \left(-\frac{1}{3}\kappa\right)^2 + \left(-\frac{1}{3}\kappa\right)^2 \tag{75}$$

$$III = \left(\frac{2}{3}\kappa\right)^3 + \left(-\frac{1}{3}\kappa\right)^3 + \left(-\frac{1}{3}\kappa\right)^3 \tag{76}$$

$$II = \left(\frac{6}{9}\right)\kappa^2 \tag{77}$$

$$III = \left(\frac{2}{9}\right)\kappa^3. \tag{78}$$

From equations (77) and (78), the relationship for the axisymmetric expansion for the (AIM) can be recovered:

$$II = \frac{3}{2}\left(\frac{4}{3}III\right)^{\frac{2}{3}}. \tag{79}$$

The matrix for the axisymmetric contraction boundary, taking $C_{1c} = 0$ is given as

$$\hat{a}_{2c-3c} = C_{2c}\begin{pmatrix} 1/6 & 0 & 0 \\ 0 & 1/6 & 0 \\ 0 & 0 & -1/3 \end{pmatrix} + C_{3c}\begin{pmatrix} 0 & 0 & 0 \\ 0 & 0 & 0 \\ 0 & 0 & 0 \end{pmatrix}. \tag{80}$$

Using relation (31), let us take $C_{2c} = \kappa$ and $C_{3c} = 1-\kappa$, therefore the invariants can be found as

$$II = \left(\frac{1}{6}\kappa\right)^2 + \left(\frac{1}{6}\kappa\right)^2 + \left(-\frac{1}{3}\kappa\right)^2 \tag{81}$$

$$III = \left(\frac{1}{6}\kappa\right)^3 + \left(\frac{1}{6}\kappa\right)^3 + \left(-\frac{1}{3}\kappa\right)^3 \tag{82}$$

$$II = \left(\frac{6}{36}\right)\kappa^2 \tag{83}$$

$$III = \left(-\frac{6}{216}\right)\kappa^3. \tag{84}$$

From equations (83) and (84) the relationship for the axisymmetric contraction for the (AIM) can be obtained:

$$II = \frac{3}{2}\left(-\frac{4}{3}III\right)^{\frac{2}{3}}. \tag{85}$$

The matrix for the two-component boundary is given as

$$\hat{a}_{2c-1c} = C_{2c}\begin{pmatrix} 1/6 & 0 & 0 \\ 0 & 1/6 & 0 \\ 0 & 0 & -1/3 \end{pmatrix} + C_{1c}\begin{pmatrix} 2/3 & 0 & 0 \\ 0 & -1/3 & 0 \\ 0 & 0 & -1/3 \end{pmatrix}. \tag{86}$$

Using relation (31), let us take $C_{2c} = \kappa$ and $C_{1c} = 1-\kappa$, therefore the invariants can be found as

$$II = \left(\frac{1}{6} - \frac{\kappa}{2}\right)^2 + \left(\frac{\kappa}{2} - \frac{1}{3}\right)^2 + \left(-\frac{1}{3}\right)^2 \tag{87}$$

$$III = \left(\frac{1}{6} - \frac{\kappa}{2}\right)^3 + \left(\frac{\kappa}{2} - \frac{1}{3}\right)^3 + \left(-\frac{1}{3}\right)^3 \tag{88}$$

$$II = \left(\frac{2}{3} + \frac{\kappa^2}{2} - \kappa\right) \tag{89}$$

$$III = \left(\frac{2}{9} - \frac{\kappa}{2} + \frac{\kappa^2}{2}\right). \tag{90}$$

From equations (89) and (90) the relationship for the two-component boundary of the (AIM) can be obtained:

$$II = \frac{2}{9} + 2III. \tag{91}$$

To obtain the limiting case of the plane strain limit we use the observation about the two matrices (86), while moving from the two-component limit toward the one-component limit the middle eigenvalue of the two-component matrix has to become zero and contribute to the major eigenvalue. Hence the relevant matrix for the plane strain limit is

$$\hat{a}_{\text{pl-strain}} = \frac{2}{3}\begin{pmatrix} 1/6 & 0 & 0 \\ 0 & 1/6 & 0 \\ 0 & 0 & -1/3 \end{pmatrix} + \frac{1}{3}\begin{pmatrix} 2/3 & 0 & 0 \\ 0 & -1/3 & 0 \\ 0 & 0 & -1/3 \end{pmatrix}, \tag{92}$$

where the C_{2c} and C_{1c} are taken as $\frac{2}{3}$ and $\frac{1}{3}$. From these relationships, the invariants can be calculated as follows:

$$II = \left(\frac{1}{3}\right)^2 + \left(-\frac{1}{3}\right)^2 = 2/9 \tag{93}$$

$$III = \left(\frac{1}{3}\right)^3 + \left(-\frac{1}{3}\right)^3 = 0. \tag{94}$$

6. Concluding remarks

The usage of the barycentric map for visualizing anisotropy of turbulence is presented in the current work. This barycentric map can be used in visualizing the normalized Reynolds stress

tensor and any anisotropic stress tensor. The computation of the barycentric coordinates at any point inside the barycentric map using relationships (32)–(34) gives the exact weighting of the limiting states at any point inside the map. This feature was not obtainable from the eigenvalue map (figure 2, left), and is reported for the first time in the field of turbulence modelling. This work allows the quantification of anisotropy for any kind of flow in terms of the scalar metrics (32)–(34). The barycentric metrics have the flexibilty of being drawn in terms a barycentric map, which is basically an equilateral map with the three limiting states at the vertices as shown in figure 3 or as a 2D plot as shown in figure 9. The metrics in the 2D plot give information about how at a particular point the anisotropic stress is behaving in terms of the limiting states.

In many recent second-order turbulence closure models, the linear algebraic constitutive relationships have been used for modeling of the unknown tensors such as the turbulent dissipation rate ϵ_{ij} and the pressure-strain correlation Φ_{ij} in the transport equation (5) for the Reynolds stress tensor; see Jovanović [3]. The function (46) can be used to obtain the correct interpolation scheme in the invariant map (AIM). The linear treatment of the barycentric coordiantes (32)–(34) eliminates the need for the introduction of nonlinear invariant variables (*II*, *III*, etc.) for visualizing the anisotropy in turbulent quantities. This new approach allows one to introduce a mathematically consistent scheme of equivalence between the various invariant maps existing in the literature in terms of (*II*, *III*) and (λ_1, λ_2) and (C_{1c}, C_{2c} and C_{3c}).

In the authors' opinion, the characterization of the turbulence states in terms of the linear matrix properties such as eigenvalues can assist in the development of mathematically consistent turbulence closure models with a minimal amount of empirical knowledge. Topics for further study will include the following tasks. Further research will focus on the construction of the linear algebraic relationships between the anisotropic Reynolds stress tensor, strain rate tensor and the dissipation tensor taking the kinematic constraints outlined in equations (23), (25) and (27); see Jovanović and Otić [13] and Jovanović et al. [12]. Finally, the performance of these models based on linear algebraic relationships and using the assumption of axisymmetry from the barycentric space will be evaluated for a wide range of different turbulent flows, not just simple homogeneous but also inhomogeneous flows.

Appendix A

Isotropic turbulence

A turbulent flow is called isotropic when, at a considered point in the flow field, its statistical quantities show no directional dependence. Hence the isotropic tensor contains all three eigenvalues equal to, e.g. $\overline{u_1u_1} = \overline{u_2u_2} = \overline{u_3u_3} = 2k/3$, and it follows from this that all eigenvalues of the corresponding anisotropy tensor $\hat{a}_{ij}$ are zero:

$$\lambda_1 = 0, \quad \lambda_2 = 0. \tag{95}$$

Axisymmetric turbulence

For axisymmetric flows, two of the fluctuating velocity components possess the same statistical quantities. Hence the Reynolds stress tensor is axisymmetric if it has two multiple eigenvalues. It is easy to see that the anisotropy tensor in the canonical form has also the same property. Using the representation expressed in equation (17), one can find that only the following three cases are allowed.

- The first component of the anisotropy tensor $\hat{a}_{ij}$ is equal to the second one:

$$\hat{a}_{11} = \hat{a}_{22} \Rightarrow \hat{a}_{ij} = \begin{pmatrix} \lambda_2 & 0 & 0 \\ 0 & \lambda_2 & 0 \\ 0 & 0 & -2\lambda_2 \end{pmatrix} \Rightarrow \lambda_1 = \lambda_2. \tag{96}$$

  This relationship (96) creates a line on the anisotropy eigenvalue domain that corresponds physically to all turbulent flows in axisymmetric contraction.
- The second and third components of the tensor $\hat{a}_{ij}$ are the same:

$$\hat{a}_{22} = \hat{a}_{33} \Rightarrow \hat{a}_{ij} = \begin{pmatrix} -2\lambda_2 & 0 & 0 \\ 0 & \lambda_2 & 0 \\ 0 & 0 & \lambda_2 \end{pmatrix} \Rightarrow \lambda_1 = -2\lambda_2. \tag{97}$$

  This relationship (97) creates a line on the anisotropy eigenvalue domain that corresponds physically to all turbulent flows in axisymmetric expansion.
- The first component of the tensor $\hat{a}_{ij}$ matches the third one:

$$\hat{a}_{11} = \hat{a}_{33} \Rightarrow \hat{a}_{ij} = \begin{pmatrix} -\lambda_2/2 & 0 & 0 \\ 0 & \lambda_2 & 0 \\ 0 & 0 & -\lambda_2/2 \end{pmatrix} \Rightarrow \lambda_1 = 0, \quad \lambda_2 = 0. \tag{98}$$

  All three components of the tensor $\hat{a}_{ij}$ have to be the same because of the ordering constraint, expressed in equation (16), is imposed on them.
  One of the most important results of this analysis is the fact that relationships (96), (97) are linear; in contrast to these relationships of axi-symmetric states (18) in the (AIM) are strongly nonlinear.

Two-component turbulence

In order for a turbulent flow to obey the two-component state of turbulence, the Reynolds stress tensor must have at least one zero eigenvalue. It follows that the corresponding anisotropy tensor, in its canonical form, is determined by equation (17) and has to contain an eigenvalue that is equal to minus one-third. The three possible situations are as follows.

- The first component of the tensor $\hat{a}_{ij}$ is equal to minus one-third:

$$\hat{a}_{11} = -\frac{1}{3} \Rightarrow \hat{a}_{ij} = \begin{pmatrix} -1/3 & 0 & 0 \\ 0 & \lambda_2 & 0 \\ 0 & 0 & 1/3 - \lambda_2 \end{pmatrix} \Rightarrow \text{No-solution.} \tag{99}$$

  This situation cannot occur physically because of the required non-increasing-order condition, expressed in equation (16), that requires $-1/3 \geq \lambda_2 \geq 1/3 - \lambda_2$. This inequality cannot be satisfied for any value of λ_2.
- The second component of the tensor $\hat{a}_{ij}$ is equal to minus one-third:

$$\hat{a}_{22} = -\frac{1}{3} \Rightarrow \hat{a}_{ij} = \begin{pmatrix} \lambda_1 & 0 & 0 \\ 0 & -1/3 & 0 \\ 0 & 0 & -\lambda_1 + 1/3 \end{pmatrix} \Rightarrow \lambda_1 = \frac{2}{3}, \quad \lambda_2 = -\frac{1}{3}. \tag{100}$$

Again, the ordering condition of equation (16) requires $\lambda_1 \geq -1/3 \geq -\lambda_1 + 1/3$, which is equivalent to the condition $\lambda_1 \geq 2/3$. The relationship expressed by equation (15) in turn shows that $\lambda_1 \leq 2/3$. Hence, the both inequalities result in the following solution: $\lambda_1 = 2/3$.

- The third component of the tensor $\hat{a}_{ij}$ is minus one-third:

$$\hat{a}_{33} = -\frac{1}{3} \Rightarrow \hat{a}_{ij} = \begin{pmatrix} \lambda_1 & 0 & 0 \\ 0 & \lambda_2 & 0 \\ 0 & 0 & -1/3 \end{pmatrix} \Rightarrow \lambda_1 = \frac{1}{3} - \lambda_2. \tag{101}$$

This result follows from the fact that the trace of the anisotropy tensor must be zero. One can conclude from this fact that the two-component limiting state of turbulence is represented in the anisotropy eigenvalue domain by a linear relationship.

$$\lambda_1 = \frac{1}{3} - \lambda_2. \tag{102}$$

Plane–strain turbulence

In order to describe the relationship between λ_1 and λ_2 of $\hat{a}_{ij}$ representing the plane–strain case of turbulence in the anisotropy eigenvalue domain, the corresponding anisotropy tensor must have at least one zero eigenvalue. Three cases might also be considered for this particular requirement.

- The first component of the tensor $\hat{a}_{ij}$ is zero:

$$\hat{a}_{11} = 0 \Rightarrow \hat{a}_{ij} = \begin{pmatrix} 0 & 0 & 0 \\ 0 & \lambda_2 & 0 \\ 0 & 0 & -\lambda_2 \end{pmatrix} \Rightarrow \lambda_1 = 0, \quad \lambda_2 = 0. \tag{103}$$

This case corresponds to the isotropic limiting state of turbulence and follows directly from the ordering requirement expressed by equation (16).

- The second component of the tensor $\hat{a}_{ij}$ is zero:

$$\hat{a}_{22} \Rightarrow \hat{a}_{ij} = \begin{pmatrix} \lambda_1 & 0 & 0 \\ 0 & 0 & 0 \\ 0 & 0 & -\lambda_1 \end{pmatrix} \Rightarrow 0 \leq \lambda_1 \leq \frac{2}{3}, \quad \lambda_2 = 0. \tag{104}$$

The resultant relationships for λ_1 and λ_2 are consequences of the normalization condition expressed by equation (15).

- The third component of the tensor $\hat{a}_{ij}$ is zero:

$$\hat{a}_{33} = 0 \Rightarrow \hat{a}_{ij} = \begin{pmatrix} \lambda_1 & 0 & 0 \\ 0 & -\lambda_1 & 0 \\ 0 & 0 & 0 \end{pmatrix} \Rightarrow \lambda_1 = 0, \quad \lambda_2 = 0. \tag{105}$$

This third case is the same as the first one.

Hence, a line represents the plane strain case of turbulence in the eigenvalue domain. The derivations above justifies the fact that the barycentric map constructed in the eigenvalue domain has all its limiting states joined by lines.

Appendix B

The relationship between the Reynolds stress tensor and the anisotropic stress tensor is given by relation (1). Let $\lambda_{r\alpha}$ be an eigenvalue of $\frac{\overline{u_i u_j}}{q^2}$ and λ_i be the corresponding eigenvalue of a_{ij}. Let the corresponding eigenvector be x_i. Then

$$a_{ij}x_i = \frac{\overline{u_i u_j}}{q^2}x_i - \frac{\delta_{ij}}{3}x_i \tag{106}$$

$$\lambda_i x_i = \lambda_{r\alpha}x_i - \frac{\delta_{ij}}{3}x_i \quad i, r\alpha = \{1, 2, 3\}, \tag{107}$$

where $\lambda_i = \lambda_\alpha - \frac{1}{3}$. It is important to note that the eigenvectors of $\frac{\overline{u_i u_j}}{q^2}$ and a_{ij} are identical. This information makes the trajectory of the $\frac{\overline{u_i u_j}}{q^2}$ and a_{ij} identical inside the barycentric map for any kind of flow.

One-component limiting state

This case corresponds to one-rank for $\frac{\overline{u_i u_j}}{q^2}$, where $\lambda_{r1} \gg \lambda_{r2} \approx \lambda_{r3}$.

$$\frac{\overline{u_i u_j}}{q^2} \cong \lambda_{r1}x_1x_1^T \cong \lambda_1 D_{1c}. \tag{108}$$

The basis matrix for the limiting state is given by

$$D_{1c} = \begin{pmatrix} 1 & 0 & 0 \\ 0 & 0 & 0 \\ 0 & 0 & 0 \end{pmatrix}. \tag{109}$$

Two-component limiting state

This case corresponds to two-rank tensor D, where $\lambda_1 \cong \lambda_2 \gg \lambda_3$.

$$\frac{\overline{u_i u_j}}{q^2} \cong \lambda_{r1}(x_1x_1^T + x_2x_2^T) \cong \lambda_{r1}D_{2c}. \tag{110}$$

The basis matrix for the limiting state is given by

$$D_{2c} = \begin{pmatrix} 1/2 & 0 & 0 \\ 0 & 1/2 & 0 \\ 0 & 0 & 0 \end{pmatrix}. \tag{111}$$

Three-component limiting state

This case corresponds to three-rank tensor D, where λ_1=λ_2=λ_3.

$$\frac{\overline{u_i u_j}}{q^2} \cong \lambda_{r1}\left(x_1x_1^T + x_2x_2^T + x_3x_3^T\right) \cong \lambda_{r1}D_{3c}. \tag{112}$$

The basis matrix for the limiting state is given by

$$D_{3c} = \begin{pmatrix} 1/3 & 0 & 0 \\ 0 & 1/3 & 0 \\ 0 & 0 & 1/3 \end{pmatrix}. \tag{113}$$

In general, the normalized Reynolds stress tensor $\frac{\overline{u_i u_j}}{q^2}$ will be a combination of these limiting cases. Expanding the tensor $\frac{\overline{u_i u_j}}{q^2}$ as a combination of these three limiting cases (one-component, two-component, three-component) as a basis gives

$$\frac{\overline{u_i u_j}}{q^2} \cong \lambda_{r1} x_1 x_1^T + \lambda_{r2} x_2 x_2^T + \lambda_{r3} x_3 x_3^T \tag{114}$$

$$\frac{\overline{u_i u_j}}{q^2} \cong (\lambda_{r1} - \lambda_{r2}) x_1 x_1^T + (\lambda_{r2} - \lambda_{r3})\left(x_1 x_1^T + x_2 x_2^T\right) + \lambda_{r3}\left(x_1 x_1^T + x_2 x_2^T + x_3 x_3^T\right) \tag{115}$$

$$\frac{\overline{u_i u_j}}{q^2} \cong (\lambda_{r1} - \lambda_{r2}) D_{1c} + (\lambda_{r2} - \lambda_{r3}) D_{2c} + (\lambda_{r3}) D_{3c}, \tag{116}$$

where $\{(\lambda_{r1} - \lambda_{r2}), (\lambda_{r2} - \lambda_{r3}), \lambda_{r3}\}$ are the coordinates of the normalized Reynolds stress tensor in the tensor basis $\{D_{1c}, D_{2c}, D_{3c}\}$. As described above the relationships between the eigenvalues of the normalized Reynolds stress tensor can be used for the classification of the normalized Reynolds stress tensor by using the coordinates of the tensor in the new basis D_{1c}, D_{2c} and D_{3c} to measure how close the normalized Reynolds stress tensor is from the generic cases of one-component, two-component and three-component states. To get a measure of anisotropy in the $\frac{\overline{u_i u_j}}{q^2}$, metrics of three different kinds of anisotropy are provided which are normalized by the magnitude of the largest eigenvalue of the tensor.

$$C_{1cr} = \frac{(\lambda_{r1} - \lambda_{r2})}{(\lambda_{r1})}, \tag{117}$$

$$C_{2cr} = \frac{(\lambda_{r2} - \lambda_{r3})}{(\lambda_{r1})}, \tag{118}$$

$$C_{3cr} = \frac{(\lambda_{r3})}{(\lambda_{r1})}. \tag{119}$$

The normalizing coefficient is chosen in a manner such that

$$C_{1cr} + C_{2cr} + C_{3cr} = 1. \tag{120}$$

The normalizing is done in such a way that all metrics $\{C_{1cr}, C_{2cr}, C_{3cr}\}$ lie in the range [0, 1]. Taking this formulation into account a barycentric map (3) can be used to characterize turbulence where the three limiting states of turbulence (one-component, two-component, three-component) represent the three vertices of the map. This is a barycentric map where at each vertex the metrics $\{C_{1cr}, C_{2cr}, C_{3cr}\}$ have coefficient 1 and then it decreases to zero for the line opposite to the vertex. Any point inside the map has local barycentric coordinates $\{C_{1cr}, C_{2cr}, C_{3cr}\}$ which helps to directly know the weightage of the three limiting states of turbulence at that point.

Acknowledgements

The authors wish to acknowledge the valuable comments made by the reviewers in improving the quality of the current work. The authors are grateful to Professor Dr. Suman Chakroborty, Dr. Oezguer Ertunc and Prof. Dr. Baensch for enlightning discussions regarding this work.

The authors are also grateful to Prof. Dr. J. L. Lumley for agreeing to review the fundamental assumptions of this work. The authors are also grateful to Dr. P.C. Weston for making the necessary english corrections required in the paper.

References

[1] Lumley, J.L. 1978, Computational modeling of turbulent flows. *Advances in Applied Mechanics*, **18**, 123–176.
[2] Lumley, J.L. and Newman, G. 1977, The return to isotropy of homogeneous turbulence. *Journal of Fluid Mechanics*, **82**, 161–178.
[3] Jovanović, J. 2004, *The Statistical Dynamics of Turbulence*. Berlin: Springer-Verlag.
[4] Kim, J., Antonia, R.A., and Browne, L.W.B. 1991, Some characteristics of small-scale turbulence in a turbulent duct flow. *Journal of Fluid Mechanics*, **233**, 369–388.
[5] Krogstad, P. and Torbergsen, L. 2000, Invariant analysis of turbulent pipe flow. *Flow, Turbulence and Combustion*, **64**, 161–181.
[6] Kwing-So Choi and John Lumley. 2001, The return to isotropy of homogenous turbulence. *Journal of Fluid Mechanics*, **436**, 59–84.
[7] Simonsen, A.J. and Krogstad, P.A. 2005, Turbulent stress invariant analysis: Clarification of existing terminology. *Physics of Fluids*, **17**, 59–84.
[8] Terentiev, L. 2005, The turbulence closure model based on linear anisotropy invariant analysis. *PhD thesis*, Technische Fakultät der Universität Erlangen-Nürnberg.
[9] Westin et al. 1997, Geometrical diffusion measures for MRI from tensor basis analysis. *Proceedings of 5th Annual ISMRM*.
[10] Schumann, U. 1977, Realizability of Reynolds stress turbulence models. *Physics of Fluids*, **20**, 721–725.
[11] Kim, J., Moin, P., and Moser, R. 1987, Turbulence statistics of a fully developed channel flow at low Reynolds number. *Journal of Fluid Mechanics*, **177**, 133–166.
[12] Jovanović, J., Otić, I., and Bradshaw, P. 2003, On the anisotropy of axisymmetric-strained turbulence in the dissipation range. *Journal of Fluid Engineering*, **125**, 401–413.
[13] Jovanović, J., and Otić, I. 2000, On the constitutive relation for the Reynolds stresses and the Prandtl–Kolmogorov hypothesis of effective viscosity in axisymmetric-strained turbulence. *ASME Journal*, **122**, 48–50.